Robust Stability Analysis for Connected Vehicle Systems

Dávid Hajdu [*], **Linjun Zhang** [**], **Tamás Insperger** [*], **and Gábor Orosz** [**]

[*] *Department of Applied Mechanics, Budapest University of Technology and Economics, Budapest, H-1111 (e-mail: hajdu@mm.bme.hu, insperger@mm.bme.hu).*
[**] *Department of Mechanical Engineering, University of Michigan, Ann Arbor, MI 48109 USA (e-mail: linjunzh@umich.edu, orosz@umich.edu).*

Abstract: For implementation in real traffic, connected vehicle systems should be designed to be robust against uncertainties arising from human-driven vehicles. Assuming that the bounds of uncertainties are known, we propose a frequency domain approach to guarantee robust string stability and to select optimal control parameters. The method is demonstrated by two case studies.

Keywords: Connected vehicle systems, plant and string stability, robustness, time delays

1. INTRODUCTION

Nowadays, the emerging wireless vehicle-to-vehicle (V2V) communication enables vehicles to monitor the motion of distant vehicles, even those beyond the line of sight. Such technology has great potentials for improving traffic efficiency, reducing fuel consumption, and enhancing vehicle safety. Cooperative adaptive cruise control (CACC) is a typical application of V2V communication, where each vehicle automatically responds to the vehicle immediately ahead based on radar while also monitoring the motion of the designated leader via V2V communication; see Kianfar et al. (2012), Alam et al. (2015), and di Bernardo et al. (2015). However, implementing CACC in real traffic is challenging since it requires vehicles of high level of autonomy to travel together, which rarely occurs in practice due to the low penetration of such vehicles.

To overcome this limitation, the concept of connected cruise control (CCC) was proposed by Zhang and Orosz (2016); Ge and Orosz (2014). CCC allows the host vehicle to monitor the motion of multiple vehicles ahead without requiring all vehicles to be equipped with range sensors or V2V communication devices, making practical implementations feasible. Mixing CCC vehicles into traffic of human-driven vehicles leads to connected vehicle systems (CVSs) where neither a designated leader nor prescribed connectivity structure is needed. To reduce the complexity for design and analysis of CVSs, Zhang and Orosz (2016) proposed a motif-based approach that allows one to design CVSs modularly and is scalable for large vehicle networks. The effects of acceleration feedback on the dynamics of CVSs were investigated by Ge and Orosz (2014) while the effects of stochastic communication delays were studied by Qin et al. (2015).

The aforementioned studies on CVSs assumed that dynamic models of all vehicles (including the human-driven vehicles) were known. However, in practice, there may exist uncertainties in dynamic models, especially for human-driven vehicles. How these modeling uncertainties affect the performance of CVSs is still an open problem. In this paper, we investigate the robustness of CVSs against modeling uncertainties.

The structure of the paper is as follows. In Sec. 2 a generalized model for connected cruise control is presented and the head-to-tail transfer function is calculated. The robust stability analysis is presented in detail in Sec. 3, including the evaluation of robust string stability. Two examples are presented in Sec. 4, where the results are summarized using robust stability diagrams. The results are concluded in Sec. 5.

2. STABILITY IN CONNECTED VEHICLE SYSTEMS

In this section, we provide a framework for connected cruise control (CCC) that includes information delays while allowing a large variety of connectivity structures. Then, plant stability and head-to-tail string stability are defined that can be used to evaluate the performance of connected vehicle systems (CVSs).

2.1 Connected Cruise Control

In Fig. 1 the CCC vehicle i (at the tail) monitors positions s_j and velocities v_j of vehicles $j = p, \dots, i-1$, where vehicle p denotes the furthest vehicle within the effective communication range of vehicle i. The symbol l_j represents the length of vehicle j while $\xi_{i,j}$ denotes the information delay between vehicles i and j. The "short-range link" (solid arrow) can be realized by human perception resulting in the human reaction time $\xi_{j,j-1} \approx 0.5$–2 [s], by radar with sensing delay $\xi_{j,j-1} \approx 0.1$–0.2 [s], or by wireless communication with delay $\xi_{j,j-1} \approx 0.1$–0.4 [s] that occurs due to intermittencies and packet drops. The "long-range

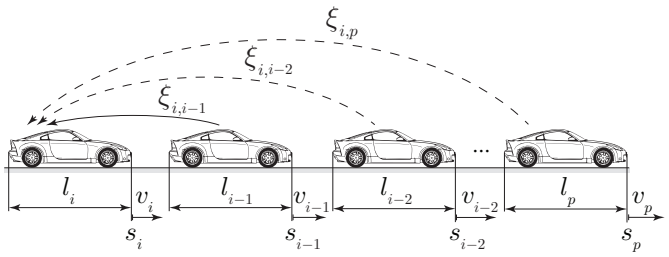

Fig. 1. A CCC vehicle i (at the tail) monitors the motion of multiple vehicles ahead, where $\xi_{j,j-1}$ are communication or sensing delays, while s_j, l_j, v_j denote the position, length and velocity of vehicle j, respectively. Arrows denote the direction of information flow. The solid link can be realized by human perception, range sensors or V2V communication, while the dashed links can only be realized by V2V communication.

links" (dashed arrows) can only be realized by wireless communication since those vehicles are beyond the line of sight.

Here, we neglect the air-drag and rolling resistance in the physics-based model given by (Ulsoy et al., 2012) and (Orosz, 2014), so that the acceleration of vehicle i is directly determined by the controller. We use the CCC framework presented by Zhang and Orosz (2016)

$$\begin{aligned}\dot{s}_i(t) &= v_i(t)\,,\\ \dot{v}_i(t) &= \sum_{j=p}^{i-1}\gamma_{i,j}\Big[\alpha_{i,j}\big(V\big(h_{i,j}(t-\xi_{i,j})\big)-v_i(t-\xi_{i,j})\big)\\ &\qquad +\beta_{i,j}\big(v_j(t-\xi_{i,j})-v_i(t-\xi_{i,j})\big)\Big]\,,\end{aligned}\tag{1}$$

where $\alpha_{i,j}$, $\beta_{i,j}$ are control gains and the connectivity structure is represented by the adjacency matrix $\mathbf{\Gamma}=[\gamma_{i,j}]$ such that

$$\gamma_{i,j}=\begin{cases}1\,, & \text{if vehicle } i \text{ uses data of vehicle } j\,,\\ 0\,, & \text{otherwise}\,.\end{cases}\tag{2}$$

In (1), the range policy function $V(h)$ gives a desired velocity based on h. Here, we use the nonlinear range policy function

$$V(h)=\begin{cases}0\,, & \text{if } h\le h_{\rm st}\,,\\ \frac{v_{\max}}{2}\Big[1-\cos\Big(\pi\frac{h-h_{\rm st}}{h_{\rm go}-h_{\rm st}}\Big)\Big]\,, & \text{if } h_{\rm st}<h<h_{\rm go}\,,\\ v_{\max}\,, & \text{if } h\ge h_{\rm go}\,,\end{cases}\tag{3}$$

which indicates that the vehicle tends to stop for small distances and aims to maintain the preset maximum speed $v_{\max}$ for large distances. In the middle range, the desired velocity monotonically increases with the distance. The nonlinearity in (3) ensures the smooth change of acceleration at $h=h_{\rm st}$ and $h=h_{\rm go}$ and hence improves the driving comfort. According to the data collected in real traffic (Orosz et al., 2010), parameters in (3) are set to be $h_{\rm st}=5$ [m], $h_{\rm go}=35$ [m], $v_{\max}=30$ [m/s].

Finally, in (1) the quantity

$$h_{i,j}(t)=\frac{1}{i-j}\Big(s_j(t)-s_i(t)-\sum_{k=j}^{i-1}l_k\Big)\tag{4}$$

denotes the average distance between vehicles i and j; cf. Fig 1. Such averaging is used such that the desired velocity $V(h_{i,j})$ is independent of the "link length" $i-j$ and also comparable for different j's.

In this paper we assume that the vehicle networks contain human-driven vehicles that are not equipped with the V2V communication devices and only perceive the behavior of the vehicle immediately ahead. When vehicle j is driven by a human driver, we assume that its dynamics is governed by the model

$$\begin{aligned}\dot{s}_j(t) &= v_j(t)\,,\\ \dot{v}_j(t) &= \alpha_{j,j-1}\big(V\big(h_{j,j-1}(t-\xi_{j,j-1})\big)-v_j(t-\xi_{j,j-1})\big)\\ &\qquad +\beta_{j,j-1}\big(v_{j-1}(t-\xi_{j,j-1})-v_j(t-\xi_{j,j-1})\big)\,,\end{aligned}\tag{5}$$

which can be obtained from (1) by setting $\gamma_{i,i-1}=1$ while $\gamma_{i,j}=0$ for all $j<i-1$. For human-driven vehicles, the parameters α, β, ξ are uncertain. Note that the CCC framework (1) ensures a unique uniform flow equilibrium

$$s_i^*(t)=v^*t-ih^*-\sum_{k=0}^{i-1}l_k\,,\quad v_i(t)\equiv v^*=V(h^*)\,,\tag{6}$$

for all i, which is independent of network size, connectivity structures, information delays, and control gains. Here the constant h^* denotes the equilibrium distance between any pair of consecutive vehicles while the constant v^* is the equilibrium velocity.

2.2 Head-to-Tail Transfer Function

To evaluate the performance of CVSs, we define the perturbations

$$\tilde{s}_i(t)=s_i(t)-s_i^*(t)\,,\quad \tilde{v}_i(t)=v_i(t)-v^*\tag{7}$$

about the uniform flow equilibrium (6) and investigate the dynamics in the vicinity of the uniform flow equilibrium. Linearizing (1) about the equilibrium (6) and transforming the result to the Laplace domain with zero initial conditions, we obtain

$$\tilde{V}_i(s)=\sum_{j=p}^{i-1}T_{i,j}(s)\tilde{V}_j(s),\tag{8}$$

where $\tilde{V}(s)$ denotes the Laplace transform of $\tilde{v}(t)$ and

$$T_{i,j}(s)=\frac{\gamma_{i,j}(s\beta_{i,j}+\varphi_{i,j})\mathrm{e}^{-s\xi_{i,j}}}{s^2+\sum_{k=p}^{i-1}\gamma_{i,k}(s\kappa_{i,k}+\varphi_{i,k})\mathrm{e}^{-s\xi_{i,k}}}\tag{9}$$

is called the *link transfer function* that acts as a dynamic gain along the link between vehicles i and j. Here, $\gamma_{i,j}$ is defined in (2) while the constants $\varphi_{i,j}$ and $\kappa_{i,j}$ are given by

$$\varphi_{i,j}=\frac{\alpha_{i,j}V'(h^*)}{i-j}\,,\quad \kappa_{i,j}=\alpha_{i,j}+\beta_{i,j}\,,\tag{10}$$

for $j=p,\dots,i-1$, where the prime denotes the derivative of function $V(h)$ in (3) with respect to h.

To evaluate plant stability and head-to-tail string stability of a vehicle network, one needs the *head-to-tail transfer function* (HTTF) $G_{n,0}(s)$, which represents the dynamic relationship between the head vehicle 0 and the tail vehicle n such that

$$\tilde{V}_n(s)=G_{n,0}(s)\tilde{V}_0(s)\,.\tag{11}$$

Note that $G_{n,0}(s)$ is determined by link transfer functions (9) and includes the dynamics of all vehicles between

vehicles 0 and n; cf. (8). Zhang and Orosz (2016) provided a systematic approach to calculate the HTTF, by using the dynamic coupling matrix

$$\mathbf{F}(s) = \mathbf{R}\big(\mathbf{T}(s) + \mathbf{I}_{n+1}\big)\mathbf{R}^{\mathrm{T}}\,, \tag{12}$$

where $\mathbf{T}(s) = [T_{i,j}(s)]$ with $i, j = 0, \ldots, n$, $\mathbf{R} = [\mathbf{0}_{n\times 1}\,, \mathbf{I}_n]$ and $\mathbf{I}_n$ denotes the n-dimensional identity matrix while $\mathbf{0}_{n\times 1}$ is an n-by-1 zero vector. Indeed, $\mathbf{F}(s)$ can be obtained by deleting the first row and last column of the matrix $\mathbf{T}(s) + \mathbf{I}_{n+1}$. Then, the HTTF is given by

$$G_{n,0}(s) = \sum_{\sigma_i \in S_n} \prod_{i=1}^{n} F_{i,\sigma_i}(s) = \frac{N(s)}{D(s)}\,, \tag{13}$$

where the sum is computed over all permutations σ_i of the set $S_n = \{1, 2, \ldots, n\}$. Formula (13) is the same as the Leibniz formula for the determinant but does not include sign changes. It can be evaluated in a symbolic or numerical mathematical software based on the determinant.

2.3 Plant Stability and Head-to-Tail String Stability

Plant stability and head-to-tail string stability are two crucial properties for CVSs. *Plant stability* indicates that the equilibrium of each vehicle in the CVS is asymptotically stable in absence of external disturbances. When disturbances are imposed on the head vehicle, a network is said to be *head-to-tail string stable* if the disturbances are attenuated when reaching the tail vehicle. Note that head-to-tail string stability allows disturbances to be amplified by some vehicles in the network. Such flexibility is particularly useful for CVSs that include human-driven vehicles, for which the dynamics cannot be designed. Indeed, plant stability is a fundamental requirement for CVSs to avoid collisions. Assuming plant stability, head-to-tail string stability is used for congestion mitigation. Here, we present conditions for plant stability and head-to-tail string stability of the linearized system by using the HTTF (13).

Note that the delays $\xi_{i,j}$ result in infinitely many poles s_i (i=1,2,...) that satisfy the characteristic equation $D(s) = 0$; cf. (13). Since the negative real parts of poles indicate the decay of initial perturbation, a vehicle network is plant stable if and only if

$$\mathrm{Re}(s_i) < 0\,, \quad i = 1, 2, \ldots\,. \tag{14}$$

Based on the HTTF (13), a sinusoidal disturbance with frequency ω from the head vehicle is amplified by the ratio $|G_{n,0}(\mathrm{j}\omega)|$ when reaching the tail vehicle. Thus, a CVS is head-to-tail string stable if and only if

$$|G_{n,0}(\mathrm{j}\omega)| < 1\,, \quad \forall \omega > 0\,, \tag{15}$$

see (Zhang and Orosz, 2016). In the following part, the robustness of CVSs against model uncertainties will be investigated by using the conditions (14) and (15).

3. ROBUST HEAD-TO-TAIL STRING STABILITY ANALYSIS

If the link transfer functions between vehicles i and j are uncertain, then it can be expressed as

$$T_{i,j}(s) = T^*_{i,j}(s) + \tilde{T}_{i,j}(s), \tag{16}$$

where $T^*_{i,j}(s)$ is the nominal transfer function and $\tilde{T}_{i,j}(s)$ represents the uncertainties due to parameter variations.

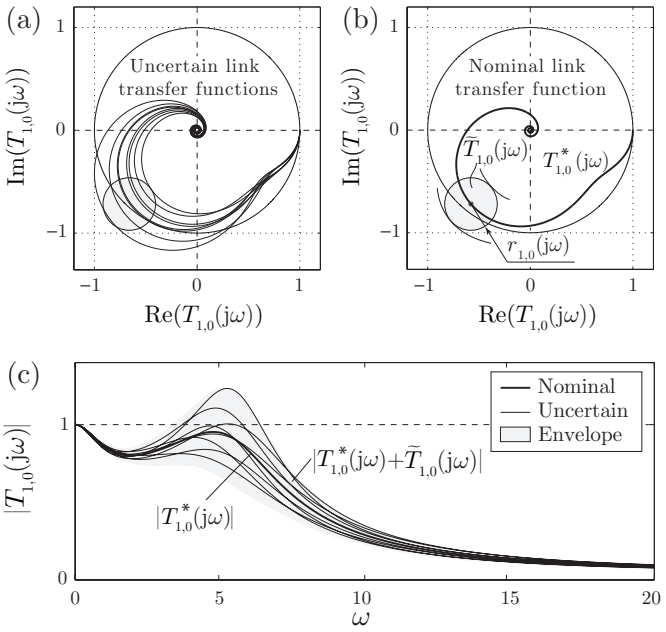

Fig. 2. Nyquist diagram (a,b) and Bode plot (c) of the link transfer function $T_{1,0}(s)$, where the parameters are $\alpha_{1,0} = 1.8\,[1/\mathrm{s}]$, $\beta_{1,0} = 2\,[1/\mathrm{s}]$, $\xi_{1,0} = 0.2\,[\mathrm{s}]$ with uncertainties 10%, 10%, 5%, respectively.

We remark that the time-varying and stochastic nature of the uncertainties are not taken into account during the analysis. For bounded perturbations for any link transfer function there exists an uncertainty radius $r_{i,j}(s) \geq 0$ such that

$$|\tilde{T}_{i,j}(s)| \leq r_{i,j}(s). \tag{17}$$

Thus, the range of uncertainties is represented by a complex disk on the Nyquist plots. Note, that by the definition of the link transfer functions (9), $T_{i,j}(0) = 1$ always holds, therefore $r_{i,j}(0) = 0$.

For example, consider a 2-vehicle scenario where the human-driven vehicle 1 reacts to vehicle 0. Then the transfer function is written as

$$T_{1,0}(s) = T^*_{1,0}(s) + \tilde{T}_{1,0}(s), \tag{18}$$

where

$$T^*_{1,0}(s) = \frac{(\beta_{1,0}s + \varphi_{1,0})\,\mathrm{e}^{-s\xi_{1,0}}}{s^2 + (\kappa_{1,0}s + \varphi_{1,0})\,\mathrm{e}^{-s\xi_{1,0}}} \tag{19}$$

is the nominal transfer function (cf. (9)) and $\tilde{T}_{1,0}(s)$ is the uncertainty. The Nyquist diagram in Fig. 2 (a) shows a bundle of transfer functions corresponding to the gain parameters $\alpha_{1,0} = 1.8\,[1/\mathrm{s}]$, $\beta_{1,0} = 2\,[1/\mathrm{s}]$, and delay $\xi_{1,0} = 0.2\,[\mathrm{s}]$ with uncertainties 10%, 10%, and 5%, respectively. The Nyquist plot in panel (b) highlights the nominal transfer function $T^*_{1,0}(\mathrm{j}\omega)$ and a circle with the radius $r_{1,0}$ represents the uncertainty radius, which encompasses the perturbation $\tilde{T}_{1,0}(\mathrm{j}\omega)$. The Bode diagram in Fig. 2 (c) plots the magnitude of the transfer functions, where the envelope corresponding to the uncertainty radii is highlighted by gray shading.

3.1 Robust string stability

As mentioned above, the control gains and delays of other vehicles are uncertain when those are driven by human

drivers. Such uncertainties affect not only the link transfer functions, but also the head-to-tail string stability of a vehicle network, and therefore they influence the strategies to select appropriate control gains for the vehicles in the string.

If the head-to-tail transfer function is uncertain, then it can be expressed by

$$G_{n,0}(s) = G^*_{n,0}(s) + \tilde{G}_{n,0}(s), \tag{20}$$

where $\tilde{G}_{n,0}(s)$ represents the complex perturbation due to parameter uncertainties around the nominal system $G^*_{n,0}(s)$. Robust stable control parameters must guarantee stability for any perturbation included in $\tilde{G}_{n,0}(s)$.

We assume that the CCC vehicle is autonomous such that the corresponding delays are known while control gains can be designed. Therefore, there exist no uncertainties in the CCC vehicle. Note that plant stability is only determined by the parameters of the CCC vehicle (see (1), $\alpha_{i,j}$, $\beta_{i,j}$, $j = p, \dots, i-1$), that is, the uncertainties arising from other vehicles have no impact on the plant stability of the CCC vehicle. Thus, we focus on the robustness of head-to-tail string stability against uncertain parameters of other vehicles.

Condition (15) for string stability including uncertainties defined by (20) reads as

$$|G^*_{n,0}(\mathrm{j}\omega) + \tilde{G}_{n,0}(\mathrm{j}\omega)| < 1, \quad \forall \omega > 0, \tag{21}$$

which must be satisfied for any perturbation $\tilde{G}_{n,0}(\mathrm{j}\omega)$. The uncertainty $\tilde{G}_{n,0}(\mathrm{j}\omega)$ depends on the propagation of the perturbation along the string of vehicles. Let us assume that the bound of uncertainties is given by a disk on the complex plane with the radius $R(\mathrm{j}\omega) \geq 0$, that is

$$|G^*_{n,0}(\mathrm{j}\omega) + \tilde{G}_{n,0}(\mathrm{j}\omega)| \leq |G^*_{n,0}(\mathrm{j}\omega)| + \underbrace{|\tilde{G}_{n,0}(\mathrm{j}\omega)|}_{\leq R(\mathrm{j}\omega)}, \tag{22}$$

cf. Fig. 2. An upper estimation of the uncertainty of the HTTF can be given by applying the triangular inequality. Thus, the uncertainty radius is defined as

$$R(\mathrm{j}\omega) := \sum_{\sigma_i \in S_n} \prod_{i=1}^{n} \left(|F^*_{i,\sigma_i}(\mathrm{j}\omega)| + r_{i,\sigma_i}(\mathrm{j}\omega) \right) - \sum_{\sigma_i \in S_n} \prod_{i=1}^{n} |F^*_{i,\sigma_i}(\mathrm{j}\omega)|, \tag{23}$$

where $\mathbf{F}^*(\mathrm{j}\omega) = \mathbf{R}(\mathbf{T}^*(\mathrm{j}\omega) + \mathbf{I}_{n+1})\mathbf{R}^{\mathrm{T}}$, $\mathbf{T}^*(\mathrm{j}\omega) = [T^*_{i,j}(\mathrm{j}\omega)]$ and $|\tilde{T}_{i,j}(\mathrm{j}\omega)| \leq r_{i,j}(\mathrm{j}\omega)$; cf. (17).

If the uncertainty radius $r_{i,j}(\mathrm{j}\omega)$ of the link transfer functions are known, then (23) can be evaluated. Based on (21)-(22) the condition for stability can be written as

$$|G^*_{n,0}(\mathrm{j}\omega)| + R(\mathrm{j}\omega) < 1, \quad \forall \omega > 0. \tag{24}$$

Note that $G^*_{n,0}(0) = 1$ and $R(0) = 0$ hold for every configuration of connected vehicle systems. Arranging the inequality and dividing by $R(\mathrm{j}\omega) > 0$, one can obtain the condition for robust string stability in the form

$$1 < S := \min_{\omega > 0} \frac{1 - |G^*_{n,0}(\mathrm{j}\omega)|}{R(\mathrm{j}\omega)}, \tag{25}$$

where S is called the safety factor. The contour curves at $S = 1$ correspond to the robust string stability boundary and $S = 0$ gives the boundary of the nominal system. Robustness can be guaranteed for any perturbation bounded by the uncertainty radius $SR(\mathrm{j}\omega)$.

4. CASE STUDIES

In this section two examples and the corresponding robust string stability diagrams are presented. It is assumed that certain vehicles in the system are driven by human drivers which utilize information only from the vehicle immediately ahead. Since each human driver has a different driving strategy, their link transfer functions are uncertain. Here uncertainties are modeled by perturbations in the control gains $\alpha_{j,j-1}$, $\beta_{j,j-1}$ and the reaction time $\xi_{j,j-1}$. Throughout the examples the generated perturbations satisfy

$$\left(\frac{\tilde{\alpha}_{j,j-1}}{\epsilon_{\alpha,j,j-1}\alpha_{j,j-1}}\right)^2 + \left(\frac{\tilde{\beta}_{j,j-1}}{\epsilon_{\beta,j,j-1}\beta_{j,j-1}}\right)^2 + \left(\frac{\tilde{\xi}_{j,j-1}}{\epsilon_{\xi,j,j-1}\xi_{j,j-1}}\right)^2 \leq 1, \tag{26}$$

where $\tilde{\alpha}_{j,j-1}$, $\tilde{\beta}_{j,j-1}$ and $\tilde{\xi}_{j,j-1}$ are the perturbations of parameters, moreover $\epsilon_{\alpha,j,j-1}$, $\epsilon_{\beta,j,j-1}$ and $\epsilon_{\xi,j,j-1}$ are the weights of the perturbations. For instance if $\epsilon_{\alpha,j,j-1} = 0.1$, then $\alpha_{j,j-1}$ is perturbed by 10% of its nominal value. Therefore the perturbed parameters must be inside a three-dimensional ellipsoid. The uncertainty radii $r_{j,j-1}(\mathrm{j}\omega)$ is then determined such that all possible transfer functions are covered by the envelope.

The measurement of real transfer functions of human drivers is a challenging task but can be done using empirical data (Safety Pilot Model Deployment, 2012).

4.1 Case 1)

The configuration of Case 1) is presented on Fig. 3, where it is assumed that the vehicle in the middle is driven by a human driver and therefore its transfer function $T_{1,0}(s)$ is uncertain. The head-to-tail transfer function can be calculated using (13), where the dynamic coupling matrix and its perturbation matrix read

$$\mathbf{F}^*(s) = \begin{bmatrix} T^*_{1,0}(s) & 1 \\ T^*_{2,0}(s) & T^*_{2,1}(s) \end{bmatrix}, \quad \tilde{\mathbf{F}}(s) = \begin{bmatrix} \tilde{T}_{1,0}(s) & 0 \\ 0 & 0 \end{bmatrix}, \tag{27}$$

and the nominal link transfer functions are

$$T^*_{1,0}(s) = \frac{(\beta_{1,0}s + \varphi_{1,0})\,\mathrm{e}^{-s\xi_{1,0}}}{s^2 + (\kappa_{1,0}s + \varphi_{1,0})\,\mathrm{e}^{-s\xi_{1,0}}}, \tag{28}$$

$$T^*_{2,1}(s) = \frac{(\beta_{2,1}s + \varphi_{2,1})\,\mathrm{e}^{-s\xi_{2,1}}}{s^2 + (\kappa_{2,1}s + \varphi_{2,1})\,\mathrm{e}^{-s\xi_{2,1}} + (\kappa_{2,0}s + \varphi_{2,0})\,\mathrm{e}^{-s\xi_{2,0}}},$$

$$T^*_{2,0}(s) = \frac{(\beta_{2,0}s + \varphi_{2,0})\,\mathrm{e}^{-s\xi_{2,0}}}{s^2 + (\kappa_{2,1}s + \varphi_{2,1})\,\mathrm{e}^{-s\xi_{2,1}} + (\kappa_{2,0}s + \varphi_{2,0})\,\mathrm{e}^{-s\xi_{2,0}}},$$

cf. (9,10). Therefore the nominal HTTF is

$$G^*_{2,0}(s) = T^*_{1,0}(s)T^*_{2,1}(s) + T^*_{2,0}(s). \tag{29}$$

Introducing perturbation in the human driver model, i.e., $T_{1,0}(s) = T^*_{1,0}(s) + \tilde{T}_{1,0}(s)$, the modified HTTF reads

$$G_{2,0}(s) = G^*_{2,0}(s) + T^*_{2,1}(s)\tilde{T}_{1,0}(s). \tag{30}$$

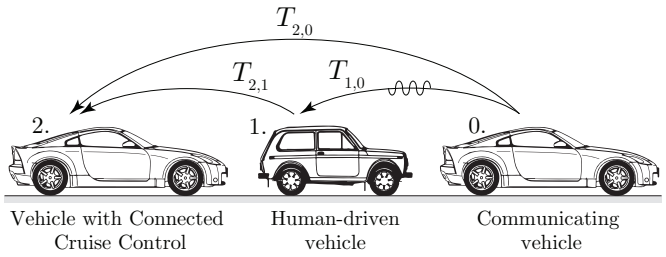

Fig. 3. Configuration of Case 1), where the transfer function $T_{1,0}(s)$ is uncertain, i.e., $T_{1,0}(s) = T^*_{1,0}(s) + \tilde{T}_{1,0}(s)$.

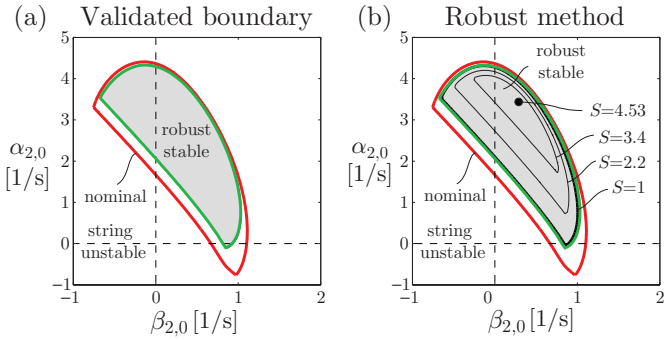

Fig. 4. Robust stability diagram of Case 1): (a) green curve indicates the results obtained from simulations (b) black curve indicates the results of the robust method for $\epsilon_{\alpha 1,0} = \epsilon_{\beta 1,0} = \epsilon_{\xi 1,0} = 0.1$. Red curves indicate the string stability boundary of the nominal system.

The last term expresses how the uncertainty propagates in the system. According to (23), the uncertainty radius becomes

$$R(\mathrm{j}\omega) = |T^*_{2,1}(\mathrm{j}\omega)|\, r_{1,0}(\mathrm{j}\omega). \tag{31}$$

The robust stability boundaries are then given by the contour lines of $S = 1$ according to (25). The most robust control gains are the ones where the safety factor is maximal.

Fig. 4 presents the stability diagram in the $(\beta_{2,0}, \alpha_{2,0})$ parameter plane with the nominal parameters $\alpha_{1,0} = \alpha_{21} = 0.6\,[1/\mathrm{s}]$, $\beta_{1,0} = \beta_{2,1} = 0.7\,[1/\mathrm{s}]$, $\xi_{1,0} = \xi_{2,1} = 0.5\,[\mathrm{s}]$, $\xi_{2,0} = 0.2\,[\mathrm{s}]$, $h^* = 20\,[\mathrm{m}]$ and $v^* = 15\,[\mathrm{m/s}]$. In the perturbed model the following uncertainties were assumed $\epsilon_{\alpha 1,0} = \epsilon_{\beta 1,0} = \epsilon_{\xi 1,0} = 0.1$ (10% perturbation). In panel (a) the shaded robust string stability domain was determined from the intersection of stability diagrams obtained from 40 independent calculations, where the perturbed parameters were taken from the boundary of the domain defined by (26). The resulting robust string stability boundary is indicated by the green curve. The boundary of the nominal system with no perturbation is denoted by the red curve. Panel (b) shows the stability diagram determined using the proposed method. For comparison the nominal and the validated boundaries are reproduced as green and red curves respectively, while the boundary of the calculated robust domain is indicated by solid black curve for safety factor $S = 1$. The difference between the green and black curves is negligible, although the latter one is in fact a conservative estimate since the uncertainty radius $r_{1,0}(\mathrm{j}\omega)$ is based on an upper estimation of the perturbation. Note, that the computation time in panel (a) significantly depends on the number of the generated stability diagrams, while panel (b) is obtained only from a single computation. Also note, that the conservativity depends on how well the envelopes cover the transfer functions. In other words, larger uncertainties can give a more conservative estimate on the uncertainty radii and finally gives a more conservative stability diagram.

Some contour curves for different values of the safety factor S are also shown in Fig. 4 (b). Larger S indicates more robust system. In this case study the maximal safety factor is $S = 4.53$. It can be seen that the most robust parameter point is not located in the center of the stable area but is shifted to larger values of $\alpha_{2,0}$ and $\beta_{2,0}$.

4.2 Case 2)

The second example presents the robust string stability diagram for the configuration shown in Fig. 5. The head-to-tail transfer function can be calculated using (13), where the dynamic coupling matrix and its perturbation matrix become

$$\mathbf{F}^*(s) = \begin{bmatrix} T^*_{1,0}(s) & 1 & 0 \\ 0 & T^*_{2,1}(s) & 1 \\ T^*_{3,0}(s) & 0 & T^*_{3,2}(s) \end{bmatrix}, \tag{32}$$

$$\tilde{\mathbf{F}}(s) = \begin{bmatrix} \tilde{T}_{1,0}(s) & 0 & 0 \\ 0 & \tilde{T}_{2,1}(s) & 0 \\ 0 & 0 & 0 \end{bmatrix}. \tag{33}$$

The nominal HTTF therefore reads

$$G^*_{n,0}(s) = T^*_{3,0}(s) + T^*_{3,2}(s) T^*_{2,1}(s) T^*_{1,0}(s). \tag{34}$$

Introducing perturbations for the human-driven vehicles as $T_{1,0}(s) = T^*_{1,0}(s) + \tilde{T}_{1,0}(s)$ and $T_{2,1}(s) = T^*_{2,1}(s) + \tilde{T}_{2,1}(s)$, the modified HTTF can be written as

$$\begin{aligned} G_{n,0}(s) = G^*_{n,0}(s) + T^*_{3,2}(s)\big(&T^*_{1,0}(s)\tilde{T}_{2,1}(s) + \\ &+ \tilde{T}_{1,0}(s) T^*_{2,1}(s) + \tilde{T}_{2,1}(s)\tilde{T}_{1,0}(s)\big). \end{aligned} \tag{35}$$

Utilizing (23), an upper estimation of the uncertainty can be given and the robust boundaries can be calculated, yielding

$$\begin{aligned} R(\mathrm{j}\omega) = |T^*_{3,2}(\mathrm{j}\omega)|\,\big(&|T^*_{1,0}(\mathrm{j}\omega)|\, r_{2,1}(\mathrm{j}\omega) + \\ &+ r_{1,0}(\mathrm{j}\omega)\,|T^*_{2,1}(\mathrm{j}\omega)| + r_{2,1}(\mathrm{j}\omega)\, r_{1,0}(\mathrm{j}\omega)\big). \end{aligned} \tag{36}$$

Fig. 6 presents the results corresponding to the nominal parameters $\alpha_{1,0} = \alpha_{2,1} = \alpha_{3,2} = 0.6\,[1/\mathrm{s}]$, $\beta_{1,0} = \beta_{2,1} = \beta_{32} = 0.7\,[1/\mathrm{s}]$, $\xi_{1,0} = \xi_{21} = \xi_{3,2} = 0.5\,[\mathrm{s}]$, $\xi_{3,0} = 0.2\,[\mathrm{s}]$, $h^* = 20\,[\mathrm{m}]$ and $v^* = 15\,[\mathrm{m/s}]$. In the perturbed model the uncertainties were assumed as $\epsilon_{\alpha 1,0} = \epsilon_{\alpha 2,1} = \epsilon_{\beta 1,0} = \epsilon_{\beta 2,1} = \epsilon_{\xi 1,0} = \epsilon_{\xi 2,1} = 0.1$. In panel (a) the validated robust string stability domain was determined from the intersection of 36 stability diagrams, so that the uncertainty of the parameters of both transfer functions $T_{1,0}(s)$ and $T_{2,0}(s)$ satisfy the equality in (26). Panel (b) shows the level curves corresponding to different safety factors, including $S = 1$ that gives the robust boundary. The largest safety factor ($S = 2.72$) is shifted to the upper boundary. Again it can be seen that the lower boundary curve is more sensitive to parameter uncertainties.

That is, in order to achieve robustness for large safety factor, CCC vehicle shall use data received directly from the lead vehicle as the short links contain uncertainties. However if the gains on the long link are much larger than

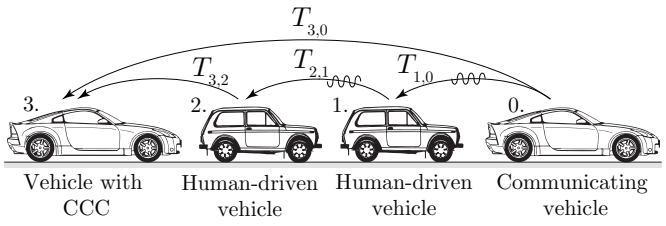

Fig. 5. Configuration of Case b), where the transfer functions $T_{1,0}(s)$ and $T_{2,1}(s)$ are uncertain, i.e., $T_{1,0}(s) = T^*_{1,0}(s) + \tilde{T}_{1,0}(s)$ and $T_{2,1}(s) = T^*_{2,1}(s) + \tilde{T}_{2,1}(s)$.

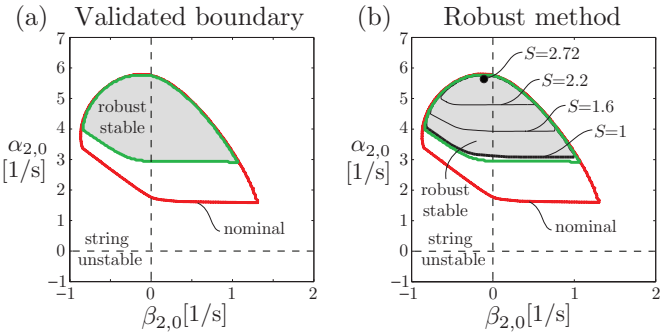

Fig. 6. Robust stability diagram of Case 2), the same notation is used as in Fig. 4.

those of the short link the system may become more prone to collisions. Therefore in practice, we need to consider the trade-off between safety and mobility.

5. CONCLUSION

In this paper we considered bounded uncertainties arising from human-driven vehicles, and proposed a frequency-domain method to design connected cruise control that ensures robust string stability. To make the calculation feasible for large vehicle networks, we derived a method that gives an estimate of robust string stability boundaries.

The method is presented for two case studies. The results show that the robustness of control parameters is not trivial. The safest point, where the safety factor is maximal, is not necessarily located at the center of the stable area, but may be close to the boundaries.

The other advantage of the technique is that it can be applied to measured frequency response functions without parameter estimation, as only an uncertainty radius must be determined.

ACKNOWLEDGEMENTS

This work was supported by the Hungarian National Science Foundation under grant OTKA-K105433 and by the National Science Foundation (Award No. 1351456).

REFERENCES

Alam, A., Mårtensson, J., and Johansson, K.H. (2015). Experimental evaluation of decentralized cooperative cruise control for heavy-duty vehicle platooning. *Control Engineering Practice*, 38, 11–25.

di Bernardo, M., Salvi, A., and Santini, S. (2015). Distributed consensus strategy for platooning of vehicles in the presence of time-varying heterogeneous communication delays. *IEEE Transactions on Intelligent Transportation Systems*, 16(1), 102–112.

Ge, J.I. and Orosz, G. (2014). Dynamics of connected vehicle systems with delayed acceleration feedback. *Transportation Research Part C*, 46, 46–64.

Kianfar, R., Augusto, B., Ebadighajari, A., Hakeem, U., Nilsson, J., Raza, A., Tabar, R.S., Irukulapati, N.V., Englund, C., Falcone, P., Papanastasiou, S., Svensson, L., and Wymeersch, H. (2012). Design and experimental validation of a cooperative driving system in the grand cooperative driving challenge. *IEEE Transactions on Intelligent Transportation Systems*, 13(3), 994–1007.

Orosz, G. (2014). Connected cruise control: modeling, delay effects, and nonlinear behavior. *Vehicle System Dynamics*, submitted.

Orosz, G., Wilson, R.E., and Stépán, G. (2010). Traffic jams: dynamics and control. *Philosophical Transactions of the Royal Society A*, 368(1928), 4455–4479.

Qin, W.B., Gomez, M.M., and Orosz, G. (2015). Stability and frequency response under stochastic communication delays with applications to connected cruise control design. In *IEEE Transactions on Intelligent Transportation Systems*, (accepted).

Safety Pilot Model Deployment (2012). *University of Michigan Transportation Research Institute.*

Ulsoy, A.G., Peng, H., and Çakmakci, M. (2012). *Automotive Control Systems.* Cambridge University Press.

Zhang, L. and Orosz, G. (2016). Motif-based design for connected vehicle systems in presence of heterogeneous connectivity structures and time delays. *IEEE Transactions on Intelligent Transportation Systems*, published online.